


## Quantum Geometric Oscillations in Two-Dimensional Flat-Band Solids

Võ Tiên Phong and E. J. Mele 

*Department of Physics and Astronomy, University of Pennsylvania, Philadelphia, Pennsylvania 19104, USA*



(Received 28 December 2022; accepted 21 April 2023; published 26 June 2023)

Two-dimensional van der Waals heterostructures can be engineered into artificial superlattices that host flat bands with significant Berry curvature and provide a favorable environment for the emergence of novel electron dynamics. In particular, the Berry curvature can induce an oscillating trajectory of an electron wave packet transverse to an applied static electric field. Though analogous to Bloch oscillations, this novel oscillatory behavior is driven entirely by quantum geometry in momentum space instead of band dispersion. While the current from Bloch oscillations can be localized by increasing field strength, the current from the geometric orbits saturates to a nonzero plateau in the strong-field limit. In nonmagnetic materials, the geometric oscillations are even under inversion of the applied field, whereas the Bloch oscillations are odd, a property that can be used to distinguish these two coexisting effects.

DOI: [10.1103/PhysRevLett.130.266601](https://doi.org/10.1103/PhysRevLett.130.266601)

Stacking or patterning atomically thin two-dimensional materials can produce translationally ordered artificial crystals with superlattice periods that greatly exceed the atomic scale [1–3]. This introduces two new generic features into their electronic behavior. First, the electronic energy bands fracture into spectrally isolated miniband manifolds that disperse weakly across a compressed Brillouin zone [4–8]. It was recognized decades ago that this feature provides a favorable environment for Bloch oscillations in quasi-one-dimensional semiconductor superlattices [9–13]. These Bloch oscillations originate from band dispersion and are a prototypical signature of quantum electron dynamics whereby a static applied electric field induces an oscillating current [14,15]. Inspired by recent progress in twistoric research, it has been suggested that analogous two-dimensional Bloch oscillations might be observable in moiré materials as well [16,17]. Second, moiré minibands can be manipulated to produce momentum-space band inversions where the orbital character of neighboring multiplets exchanges [18–22]. This introduces a fundamentally different type of oscillation driven by quantum geometry encoded in the momentum-space Berry curvature with important consequences for transport. Unlike Bloch oscillations, these *geometric oscillations* do not exist in one dimension, and are especially relevant to modern topological moiré materials.

In this Letter, we elucidate the characteristics of these geometric oscillations in nonmagnetic crystals both in the semiclassical description and in the Wannier-Stark framework. We find that the frequencies for both Bloch and geometric oscillations share the same dependence on the applied field. However, the sizes and shapes of the orbits are drastically different in the two cases. For the conventional Bloch oscillations, the direction depends sensitively on the orientation of the applied field relative to the

symmetry axes of the crystal, and the amplitude decays inversely proportionally to the field magnitude. On the other hand, the geometric oscillations always propagate transverse to the applied field, and their amplitudes are characteristically independent of the electric field magnitude. In ultracold optical lattices, the geometric influence on wave packet dynamics has already been used to map the Berry curvature [23,24]. However, in solid-state media, directly measuring wave packet dynamics is difficult; thus, we focus on transport signatures instead. In transport, the incompressibility of geometric orbits translates to a generic finite residual drift Hall current at strong fields, in stark contrast to the vanishing drift current originating from Bloch oscillations due to Wannier-Stark localization [25–29]. Thus, the diagnostic of Bloch oscillations via measuring negative differential conductance breaks down for the geometric oscillations [30]. Instead, the signature of geometric oscillations is a saturation of the drift Hall currents as field strength increases. Furthermore, the drift currents from Bloch oscillations change sign when the applied field is inverted, while the drift currents from geometric oscillations are invariant under field inversion, a property that allows these two currents to be distinguished when they coexist. This property was also noted in Ref. [23]. In addition to being a fascinating demonstration of the quantum geometric nature of electrons in crystalline solids, observing these geometric oscillations would be an important step toward the ambitious goal of eventually deploying these oscillatory currents as radiation sources.

We start with the dynamics of a wave packet in an isolated  $n$ th band governed by the semiclassical equations [31–33]

$$\hbar\dot{\mathbf{k}} = -e\mathbf{E}, \quad \hbar\dot{\mathbf{r}}_n = \nabla_{\mathbf{k}}\epsilon_{n,\mathbf{k}} + \hbar\dot{\mathbf{k}} \times \boldsymbol{\Omega}_{n,\mathbf{k}}, \quad (1)$$

where  $\varepsilon_{n,\mathbf{k}}$  and  $\mathbf{\Omega}_{n,\mathbf{k}} = \Omega_{n,\mathbf{k}} \hat{\mathbf{e}}_z$  are the band dispersion and Berry curvature. Both of these functions are real and  $\mathbf{k}$ -periodic, and thus can be expanded in Fourier series  $\varepsilon_{n,\mathbf{k}} = \sum_{\mathbf{a}_i} e^{i\mathbf{a}_i \cdot \mathbf{k}} \tilde{\varepsilon}_{n,\mathbf{a}_i}$  and  $\mathbf{\Omega}_{n,\mathbf{k}} = \sum_{\mathbf{a}_i} e^{i\mathbf{a}_i \cdot \mathbf{k}} \tilde{\mathbf{\Omega}}_{n,\mathbf{a}_i}$ , and  $\mathbf{a}_i$  is a lattice translation vector. Integrating  $\dot{\mathbf{r}}_n$  with respect to  $t$ , we obtain three distinct contributions:

$$\begin{aligned} \mathbf{r}_{\text{drift}}(t) &= \frac{t}{\hbar} \sum_{\mathbf{a}_i \cdot \mathbf{E} \neq 0} e^{i\mathbf{a}_i \cdot \mathbf{k}_0} [i\mathbf{a}_i \tilde{\varepsilon}_{n,\mathbf{a}_i} - e\mathbf{E} \times \tilde{\mathbf{\Omega}}_{n,\mathbf{a}_i}], \\ \mathbf{r}_{\text{Bloch}}(t) &= \sum_{\mathbf{a}_i \cdot \mathbf{E} \neq 0} e^{i\mathbf{a}_i \cdot \mathbf{k}_0} [1 - e^{-ie\mathbf{a}_i \cdot \mathbf{E}t/\hbar}] \frac{\mathbf{a}_i \tilde{\varepsilon}_{n,\mathbf{a}_i}}{e\mathbf{a}_i \cdot \mathbf{E}}, \\ \mathbf{r}_{\text{geom}}(t) &= i \sum_{\mathbf{a}_i \cdot \mathbf{E} \neq 0} e^{i\mathbf{a}_i \cdot \mathbf{k}_0} [1 - e^{-ie\mathbf{a}_i \cdot \mathbf{E}t/\hbar}] \frac{\mathbf{E} \times \tilde{\mathbf{\Omega}}_{n,\mathbf{a}_i}}{\mathbf{a}_i \cdot \mathbf{E}}. \end{aligned} \quad (2)$$

The drift term includes a topological contribution that is directly proportional to the Chern number  $\mathcal{C} = \int (d^2\mathbf{k}/2\pi) \Omega_n(\mathbf{k}) \propto \tilde{\mathbf{\Omega}}_{n,0}$ . Thus, it makes sense that this term is a constant drift instead of an oscillation, because it transports electrons from one edge to another. All the other terms in  $\mathbf{r}_{\text{drift}}(t)$  occur along lines where the electric field is perpendicular to a lattice vector  $\mathbf{a}_i$ . This is because these components experience no acceleration due to the electric field, and thus their contributions to the velocity are constant. The Bloch oscillating term  $\mathbf{r}_{\text{Bloch}}(t)$  is caused by the usual band dispersion. In general, it has a complicated directional dependence. The crystal momentum monotonically traces out a straight path in  $\mathbf{k}$  along the direction of  $\mathbf{E}$ . At each  $\mathbf{k}$  point, the velocity points along the direction of the gradient of the dispersion. The amplitude of these orbits diverges as  $E^{-1}$ . That is, at weak field strengths, the amplitude is macroscopic, much larger than the mean free path. So a scattering event likely occurs before an electron has time to execute a complete orbit, making Bloch oscillations notoriously difficult to observe. In contrast, the geometric term  $\mathbf{r}_{\text{geom}}(t)$  has a simple directional dependence, pointing always orthogonally to  $\mathbf{E}$ . The amplitude of this term is characteristically *independent* of the magnitude of  $\mathbf{E}$ . Meanwhile, the oscillation frequency increases with  $E$ . In what follows, we will ignore the drift contributions and focus entirely on the oscillatory behavior.

The consequences of geometric oscillations can be interrogated from a complementary perspective using the Wannier-Stark formalism [14,34–37], which offers real-space insights absent in the semiclassical description. We begin with a tight-binding lattice that contains  $\sigma$  atomic orbitals located at  $\boldsymbol{\tau}_\sigma$  within a unit cell, denoted by  $|A_{\mathbf{a}_i,\sigma}\rangle$ , and an electric field  $\mathbf{E}$ . These orbitals are assumed to be site-localized such that the position operator  $\hat{\mathbf{r}}$  is diagonal in this basis. In momentum space with  $|\varphi_{\mathbf{k},\sigma}\rangle = \mathcal{N}^{-\frac{1}{2}} \sum_{\mathbf{a}_i} |A_{\mathbf{a}_i,\sigma}\rangle e^{i\mathbf{k} \cdot (\mathbf{a}_i + \boldsymbol{\tau}_\sigma)}$ , where  $\mathcal{N}$  is the number of unit cells, the Hamiltonian is [38,39]

$$\hat{\mathcal{H}} = \sum_{\mathbf{k},\sigma',\sigma} |\varphi_{\mathbf{k},\sigma'}\rangle [\mathcal{H}_0^{\sigma',\sigma}(\mathbf{k}) + i\delta_{\sigma',\sigma} e\mathbf{E} \cdot \nabla_{\mathbf{k}}] \langle \varphi_{\mathbf{k},\sigma} |, \quad (3)$$

where  $\mathcal{H}_0^{\sigma',\sigma}(\mathbf{k}) = \sum_{\mathbf{a}_i} e^{i\mathbf{k} \cdot (\mathbf{a}_i + \boldsymbol{\tau}_{\sigma'} - \boldsymbol{\tau}_\sigma)} \langle A_{0,\sigma'} | \hat{\mathcal{H}}_0 | A_{\mathbf{a}_i,\sigma} \rangle$ , and  $\hat{\mathcal{H}}_0$  is the Hamiltonian without electric field. The gradient acts to the right. We now project this Hamiltonian to an *isolated* energy band of interest with eigenstates  $|\psi_{\mathbf{k}}\rangle$  and energies  $\varepsilon_{\mathbf{k}}$  satisfying  $\mathcal{H}_0(\mathbf{k})\chi_{\mathbf{k}} = \varepsilon_{\mathbf{k}}\chi_{\mathbf{k}}$  and  $|\psi_{\mathbf{k}}\rangle = \sum_{\sigma} \chi_{\mathbf{k},\sigma} |\varphi_{\mathbf{k},\sigma}\rangle$ . The band index is implicit. This band projection is permissible when there at least exist sizable gaps between the band of interest and other energy bands so that Zener tunneling can be neglected [40]. We find [41–43]

$$\hat{\mathcal{H}}_{\text{eff}} = \sum_{\mathbf{k}} |\psi_{\mathbf{k}}\rangle [\varepsilon_{\mathbf{k}} + e\mathbf{E} \cdot \mathcal{A}_{\mathbf{k}} + ie\mathbf{E} \cdot \nabla_{\mathbf{k}}] \langle \psi_{\mathbf{k}} |, \quad (4)$$

where  $\mathcal{A}_{\mathbf{k}} = i\chi_{\mathbf{k}}^\dagger \nabla_{\mathbf{k}} \chi_{\mathbf{k}}$  is the Berry connection. For the Berry connection to be well defined,  $\chi_{\mathbf{k}}$  must be differentiable, which can always be chosen for Chern-trivial bands; we assume this throughout, since the absence of a Chern number actually makes the oscillatory behavior clearer. Also, although the Berry connection is not gauge invariant, we will demonstrate that the results are indeed gauge invariant.

The single-band effective Hamiltonian in Eq. (4) can be diagonalized exactly by solving the partial differential equation  $\mathcal{E}\Psi_{\mathbf{k}} = [\varepsilon_{\mathbf{k}} + e\mathbf{E} \cdot \mathcal{A}_{\mathbf{k}} + ie\mathbf{E} \cdot \nabla_{\mathbf{k}}]\Psi_{\mathbf{k}}$ . Requiring  $\Psi_{\mathbf{k}} = \Psi_{\mathbf{k}+\mathbf{G}}$ , we can write  $\Psi_{\mathbf{k}} = \sum_{\mathbf{a}_i} e^{i\mathbf{k} \cdot \mathbf{a}_i} \tilde{\Psi}_{\mathbf{a}_i}$  and find that the eigenvalue problem can be cast in the form of a matrix equation:

$$\sum_{\mathbf{a}_i'} [\tilde{\varepsilon}_{\mathbf{a}_i - \mathbf{a}_i'} + e\mathbf{E} \cdot \tilde{\mathcal{A}}_{\mathbf{a}_i - \mathbf{a}_i'}] \tilde{\Psi}_{\mathbf{a}_i'} - e\mathbf{E} \cdot \mathbf{a}_i \tilde{\Psi}_{\mathbf{a}_i} = \mathcal{E} \tilde{\Psi}_{\mathbf{a}_i}. \quad (5)$$

This is an  $\mathcal{N} \times \mathcal{N}$  matrix equation with  $\mathcal{N}$  eigenvalues. If  $\Psi_{\mathbf{k}}$  is an eigenstate with eigenvalue  $\mathcal{E}$ , then  $\Psi_{\mathbf{k}} e^{-i\mathbf{k} \cdot \mathbf{a}_i}$  is also an eigenstate, not necessarily independent, with eigenvalue  $\mathcal{E} + e\mathbf{E} \cdot \mathbf{a}_i$ . When  $\mathbf{E} \cdot \mathbf{a}_i \neq 0$  for any nonzero  $\mathbf{a}_i$ , then a complete orthonormal set of solutions can be written exactly as  $\langle \psi_{\mathbf{k}} | \Psi_{\mathbf{a}_i} \rangle = \Psi_{\mathbf{k},\mathbf{a}_i} = \mathcal{N}^{-\frac{1}{2}} \exp(i\theta_{\mathbf{k}} - i\mathbf{k} \cdot \mathbf{a}_i)$  with energies  $\mathcal{E}_{\mathbf{a}_i} = e\mathbf{E} \cdot \mathbf{a}_i + \tilde{\varepsilon}_0 + e\mathbf{E} \cdot \tilde{\mathcal{A}}_0$ , where  $\theta_{\mathbf{k}} = \sum_{\mathbf{a}_i \neq 0} [\tilde{\varepsilon}_{\mathbf{a}_i} + e\mathbf{E} \cdot \tilde{\mathcal{A}}_{\mathbf{a}_i}] [ie\mathbf{E} \cdot \mathbf{a}_i]^{-1} e^{i\mathbf{k} \cdot \mathbf{a}_i}$ . It is clear that  $\theta_{\mathbf{k}}$  is a real function. We observe that the energy levels form a discrete ladder with spacing given by  $e\mathbf{a}_i \cdot \mathbf{E}$ ; this is the two-dimensional counterpart to the usual Wannier-Stark ladder [14]. The Berry connection plays no role in the relative spacing between ladder rungs; it only affects the zero of energy, which we can shift so that  $\mathbf{a}_i = \mathbf{0}$ ,  $\mathcal{E}_0 = 0$ .

The wave function  $|\Psi_{\mathbf{a}_i}\rangle$  is centered inside unit cell  $\mathbf{a}_i$  with spatial spread  $\langle \delta \hat{\mathbf{r}}^2 \rangle = \langle \hat{\mathbf{r}}^2 \rangle - \langle \hat{\mathbf{r}} \rangle^2$  given by

$$\langle \delta \hat{\mathbf{r}}^2 \rangle = \frac{1}{\mathcal{N}} \sum_{\mathbf{k}} |i\nabla_{\mathbf{k}} \chi_{\mathbf{k}} - \chi_{\mathbf{k}} \nabla_{\mathbf{k}} \theta_{\mathbf{k}}|^2 - \frac{1}{\mathcal{N}^2} \left| \sum_{\mathbf{k}} \mathcal{A}_{\mathbf{k}} \right|^2. \quad (6)$$

It is straightforward to check that this quantity is gauge invariant under  $\chi_{\mathbf{k}} \mapsto e^{i\theta_{\mathbf{k}}} \chi_{\mathbf{k}}$ , which must be the case, since energy eigenstates should have a well-defined probability density. For a one-band model,  $\chi_{\mathbf{k}} = 1$ ; so the width of  $|\Psi_{\mathbf{a}_i}\rangle$  is controlled by  $|\sum_{\mathbf{k}} \nabla_{\mathbf{k}} \theta_{\mathbf{k}}|^2$ , which vanishes as  $E^{-2}$ , since  $\theta_{\mathbf{k}}$  only depends on the energy dispersion in this case. Therefore, in a one-band model, the wave function becomes completely spatially localized in the strong-field limit, leading to Stark-Wannier localization. In a many-band model, the Berry connection obstructs this localization. In the large- $E$  limit, the energy eigenstates can retain a finite  $E$ -independent width. As argued in Ref. [44], this means that with the Berry connection, the matrix elements of the current operator between adjacent eigenstates need not vanish in the large-field limit, leading to a residual current in that regime.

A connection to the semiclassical description can be found by studying the dynamics of a wave packet initially localized at  $\mathbf{a}_j$  and centered around crystal momentum  $\mathbf{k}_0$ :

$$|\phi_{\mathbf{a}_j, \mathbf{k}_0}\rangle = \frac{1}{A} \sum_{\mathbf{a}_i} \exp \left[ i\mathbf{k}_0 \cdot \mathbf{a}_i - \frac{|\mathbf{a}_i - \mathbf{a}_j|^2}{2a^2} \right] |W_{\mathbf{a}_i}\rangle, \quad (7)$$

where  $a$  is the spatial width of the wave packet, assumed to be larger than the lattice spacing to make the theory analytically controlled,  $A \approx \sqrt{\pi a^2 / V}$ , and  $|W_{\mathbf{a}_i}\rangle = (1/\sqrt{N}) \sum_{\mathbf{k}} e^{-i\mathbf{k} \cdot \mathbf{a}_i} |\psi_{\mathbf{k}}\rangle$  are band-projected exponentially localized Wannier functions. To calculate time evolution, we need  $\hat{U}(t) = \sum_{\mathbf{a}_i} |\Psi_{\mathbf{a}_i}\rangle \langle \Psi_{\mathbf{a}_i}| e^{-ie\mathbf{E} \cdot \mathbf{a}_i t / \hbar}$ , which has the matrix elements

$$\langle W_{\mathbf{a}'_i} | \hat{U}(t) | W_{\mathbf{a}_i} \rangle = \frac{1}{N} \sum_{\mathbf{k}} e^{i\theta_{\mathbf{k}(t)} - i\theta_{\mathbf{k}} + i\mathbf{k}(t) \cdot \mathbf{a}'_i - i\mathbf{k} \cdot \mathbf{a}_i}, \quad (8)$$

where  $\mathbf{k}(t) = \mathbf{k} - e\mathbf{E}t/\hbar$ , which reproduces the acceleration theorem requiring  $\mathbf{k} \mapsto \mathbf{k} - e\mathbf{E}t/\hbar$ . We calculate the time evolution of the position operator  $\langle \hat{\mathbf{r}}(t) \rangle$  expanded in the Wannier basis [45]:

$$\begin{aligned} \langle \hat{\mathbf{r}}(t) \rangle &= \sum_{\mathbf{a}'_i, \mathbf{a}''_i} \langle \phi_{\mathbf{a}_j, \mathbf{k}_0} | \hat{U}^\dagger(t) | W_{\mathbf{a}'_i} \rangle \\ &\quad \times \langle W_{\mathbf{a}'_i} | \hat{\mathbf{r}} | W_{\mathbf{a}''_i} \rangle \langle W_{\mathbf{a}''_i} | \hat{U}(t) | \phi_{\mathbf{a}_j, \mathbf{k}_0} \rangle, \\ \langle W_{\mathbf{a}'_i} | \hat{\mathbf{r}} | W_{\mathbf{a}''_i} \rangle &= \frac{1}{N} \sum_{\mathbf{k}} \mathcal{A}_{\mathbf{k}} e^{i\mathbf{k} \cdot (\mathbf{a}'_i - \mathbf{a}''_i)} + \mathbf{a}''_i \delta_{\mathbf{a}'_i, \mathbf{a}''_i}. \end{aligned} \quad (9)$$

Then, differentiating  $\partial_t \langle \hat{\mathbf{r}}(t) \rangle$ , we find

$$\hbar \frac{d\langle \hat{\mathbf{r}}(t) \rangle}{dt} = \nabla_{\mathbf{k}} \varepsilon_{\mathbf{k}(t)} - e\mathbf{E} \times \boldsymbol{\Omega}_{\mathbf{k}(t)}, \quad (10)$$

which recovers exactly Eq. (1).

We now assess the consequences of Bloch and geometric oscillations on transport properties. To do this, we use the steady-state Boltzmann equation to find the occupation

function  $f_{\mathbf{k}} = \sum_{\mathbf{a}_i} (1 - ie\mathbf{E} \cdot \mathbf{a}_i \tau / \hbar)^{-1} \tilde{f}_{\mathbf{a}_i}^0 e^{i\mathbf{k} \cdot \mathbf{a}_i}$  from the equilibrium occupation  $f_{\mathbf{k}}^0 = \sum_{\mathbf{a}_i} \tilde{f}_{\mathbf{a}_i}^0 e^{i\mathbf{k} \cdot \mathbf{a}_i}$ , where  $\tau$  is the relaxation time, which we assume is a constant [16,46,47]. We find two distinct regimes:

$$f_{\mathbf{k}} \approx f_{\mathbf{k}}^0 + \frac{e\tau}{\hbar} \mathbf{E} \cdot \nabla_{\mathbf{k}} f_{\mathbf{k}}^0 \quad (11)$$

for small  $\mathbf{E}$ , and

$$f_{\mathbf{k}} \approx \sum_{\mathbf{E} \cdot \mathbf{a}_i = 0} \tilde{f}_{\mathbf{a}_i}^0 e^{i\mathbf{k} \cdot \mathbf{a}_i} + \frac{i\hbar}{e\tau} \sum_{\mathbf{E} \cdot \mathbf{a}_i \neq 0} (\mathbf{E} \cdot \mathbf{a}_i)^{-1} \tilde{f}_{\mathbf{a}_i}^0 e^{i\mathbf{k} \cdot \mathbf{a}_i} \quad (12)$$

for large  $\mathbf{E}$ . The steady-state drift currents are given by  $\mathbf{J}_{\text{Bloch}} = -(e/\hbar) \int [d^2\mathbf{k}/(2\pi)^2] f_{\mathbf{k}} \nabla_{\mathbf{k}} \varepsilon_{\mathbf{k}}$  and  $\mathbf{J}_{\text{geom}} = (e^2/\hbar) \int [d^2\mathbf{k}/(2\pi)^2] \mathbf{E} \times (f_{\mathbf{k}} \boldsymbol{\Omega}_{\mathbf{k}})$ . Assuming time-reversal symmetry in the absence of an external field throughout this work, we have  $f_{\mathbf{k}}^0 = f_{-\mathbf{k}}^0$  and  $\tilde{f}_{\mathbf{a}_i}^0 = \tilde{f}_{-\mathbf{a}_i}^0$ . Using this, we see that the first terms in Eqs. (11) and (12) are even under time reversal, while the second terms are odd. Since both  $\nabla_{\mathbf{k}} \varepsilon_{\mathbf{k}}$  and  $\boldsymbol{\Omega}_{\mathbf{k}}$  are odd under time reversal, only the odd components of the occupation function contribute to the current density. We observe further that the  $\mathcal{T}$ -odd components of  $f_{\mathbf{k}}$  are also odd under  $\mathbf{E} \mapsto -\mathbf{E}$  in both the small and large field limits. This means that  $\mathbf{J}_{\text{Bloch}}$  is generically odd under  $\mathbf{E}$ -inversion, while  $\mathbf{J}_{\text{geom}}$  is even under  $\mathbf{E}$ -inversion in these two regimes. This symmetry property was also found by the authors of Ref. [23]. In steady state, the currents are time independent, so Bloch and geometric oscillations do not manifest explicitly; instead, their effects show up in the scaling behaviors of these currents [48].

In the small-field limit, at lowest order,  $|\mathbf{J}_{\text{Bloch}}|$  scales as  $E = |\mathbf{E}|$ ; this is the usual Drude regime where current varies linearly with applied voltage. On the other hand,  $|\mathbf{J}_{\text{geom}}|$  scales as  $E^2$  at small fields because the occupation function contributes one factor of  $E$ , and the curvature-induced velocity contributes another. This is the conventional second-order nonlinear Hall effect [49,50]. If symmetry forbids the second-order signal, then the nonlinear Hall effect is generically activated at higher orders in  $E$ . Regardless, this small- $E$  regime contains no information about the oscillatory behavior predicted by the semiclassical equations. To observe such an oscillation, we must go to the large-field regime, where the scaling behavior is completely different. Here, we have

$$\begin{aligned} \mathbf{J}_{\text{Bloch}} &\approx -\frac{i}{\tau} \sum_{\mathbf{E} \cdot \mathbf{a}_i \neq 0} \tilde{f}_{\mathbf{a}_i}^0 \int \frac{d^2\mathbf{k}}{(2\pi)^2} \frac{\nabla_{\mathbf{k}} \varepsilon_{\mathbf{k}}}{\mathbf{E} \cdot \mathbf{a}_i} e^{i\mathbf{k} \cdot \mathbf{a}_i}, \\ \mathbf{J}_{\text{geom}} &\approx \frac{ie}{\tau} \sum_{\mathbf{E} \cdot \mathbf{a}_i \neq 0} \tilde{f}_{\mathbf{a}_i}^0 \int \frac{d^2\mathbf{k}}{(2\pi)^2} \frac{\hat{\mathbf{e}}_{\mathbf{E}} \times \boldsymbol{\Omega}_{\mathbf{k}}}{\hat{\mathbf{e}}_{\mathbf{E}} \cdot \mathbf{a}_i} e^{i\mathbf{k} \cdot \mathbf{a}_i}, \end{aligned} \quad (13)$$

where  $\hat{\mathbf{e}}_{\mathbf{E}} = \mathbf{E}/E$ .  $\mathbf{J}_{\text{Bloch}}$  decays as  $E^{-1}$ . On the other hand,  $\mathbf{J}_{\text{geom}}$  generically reaches a constant residual current density that is independent of  $E$ . If this residual current is nonzero, it means that complete Wannier-Stark localization is impossible, since the current does not vanish in large  $E$ .



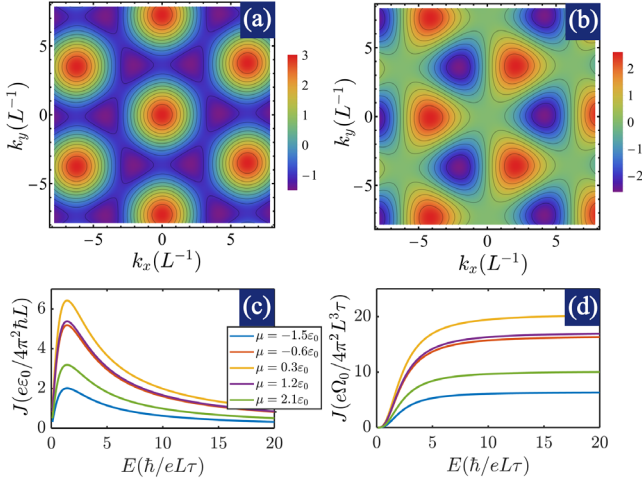


FIG. 1. Bloch and geometric oscillations in model system. (a), (b) Band structure and Berry curvature of model system defined in the text. This system respects  $\mathcal{T}$  symmetry and  $C_{3z}$  rotation symmetry. The Berry curvature is even (odd) under  $\mathcal{M}_y$  ( $\mathcal{M}_x$ ) mirror exchange. (c)  $\mathbf{J}_{\text{Bloch}} = J\hat{\mathbf{e}}_x$  as a function of applied electric field  $\mathbf{E} = E\hat{\mathbf{e}}_x$  for various values of the chemical potential. The onset of negative differential conductance occurs around  $E \approx 1$ . (d)  $\mathbf{J}_{\text{geom}} = J\hat{\mathbf{e}}_y$  as a function of the applied electric field  $\mathbf{E} = E\hat{\mathbf{e}}_x$  for various values of the chemical potential. In this case, there is no negative differential conductance; instead, the current plateaus at some finite value for large  $E$ .

Therefore, a signature of geometric quantum oscillations is *vanishing* differential Hall conductance in the infinite- $E$  limit. This is the geometric analog to negative *longitudinal* differential conductance that is believed to give an unambiguous signature of the usual Bloch oscillations [30,44,51]. When  $\mathbf{E}$  crosses over from the regime of quadratically amplified  $\mathbf{J}_{\text{geom}}$  to the regime of constant  $\mathbf{J}_{\text{geom}}$ , this can be accompanied by a region in  $E$  space where negative differential Hall conductance is observed, although this is not guaranteed in general.

The physics discussed above can be illustrated using a simple model with energy dispersion  $\varepsilon(\mathbf{k}) = \varepsilon_0 \sum_{i=1}^3 \cos(\mathbf{k} \cdot \mathbf{a}_i)$  and Berry curvature  $\mathbf{\Omega}(\mathbf{k}) = \Omega_0 \hat{\mathbf{e}}_z \sum_{i=1}^3 \sin(\mathbf{k} \cdot \mathbf{a}_i)$ , where  $\mathbf{a}_1 = L[-\frac{1}{2}, (\sqrt{3}/2)]$ ,  $\mathbf{a}_2 = L(1, 0)$ , and  $\mathbf{a}_3 = -\mathbf{a}_1 - \mathbf{a}_2$ . As shown in Figs. 1(a) and 1(b), this model respects time-reversal symmetry as well as threefold rotation symmetry; the Berry curvature is even (odd) under mirror exchange about the  $x$  axis ( $y$  axis). It importantly breaks inversion symmetry, because otherwise, in combination with time-reversal symmetry, the Berry curvature would be required to vanish. From a symmetry point of view, this model is equivalent to monolayer graphene with a sublattice staggered potential. If one projects to the valence or conduction band in that system and keeps only the first star of Fourier harmonics in the energy dispersion and Berry curvature, one would obtain the present toy model.

Applying an electric field along the  $x$  direction, we find that  $\mathbf{J}_{\text{Bloch}}$  points entirely along  $\mathbf{E}$ , with a magnitude that

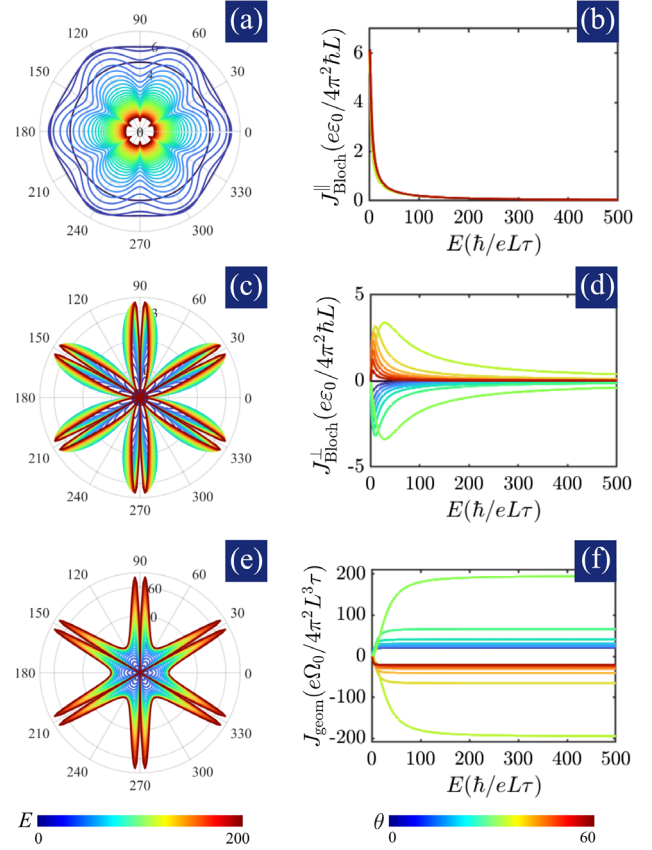


FIG. 2. Angular anisotropy of currents. Polar plots of the magnitudes (a)  $|J_{\text{Bloch}}^{\parallel}|$ , (c)  $|J_{\text{Bloch}}^{\perp}|$ , and (e)  $|J_{\text{geom}}|$  with the angle coordinate corresponding to the angle of  $\mathbf{E}$ , the radius coordinate corresponding to the current magnitude, and color corresponding to the magnitude of  $\mathbf{E}$ . Line plots showing (b)  $J_{\text{Bloch}}^{\parallel}$ , (d)  $J_{\text{Bloch}}^{\perp}$ , and (f)  $J_{\text{geom}}$  as functions of  $E$  for different values of  $0^\circ \leq \theta \leq 60^\circ$ . While  $J_{\text{Bloch}}^{\parallel}$  is only weakly dependent on  $\theta$ , the transverse currents  $J_{\text{Bloch}}^{\perp}$  and  $J_{\text{geom}}$  feature strong angular anisotropy. However,  $J_{\text{Bloch}}^{\perp}$  is even under  $\mathbf{E}$ -inversion, while  $J_{\text{geom}}$  is odd under  $\mathbf{E}$ -inversion.

first increases linearly with  $E$ , peaks around  $eE\tau/\hbar \approx 1$ , and then monotonically decreases with further increases in  $E$ , as shown in Fig. 1(c). On the other hand,  $\mathbf{J}_{\text{geom}}$  is aligned orthogonally to  $\mathbf{E}$  with a magnitude that increases rapidly as a nonlinear power law at small  $E$ , then changes concavity and approaches asymptotically a constant limit at large  $E$ , as shown in Fig. 1(d). Next, we assess the dependence of the currents on the direction of  $\mathbf{E}$ , which we write as  $\mathbf{E} = E \cos \theta \hat{\mathbf{e}}_x + E \sin \theta \hat{\mathbf{e}}_y$ . We decompose  $\mathbf{J}_{\text{Bloch}} = J_{\text{Bloch}}^{\parallel} \hat{\mathbf{e}}_E + J_{\text{Bloch}}^{\perp} \hat{\mathbf{e}}_z \times \hat{\mathbf{e}}_E$  and  $\mathbf{J}_{\text{geom}} = J_{\text{geom}} \hat{\mathbf{e}}_z \times \hat{\mathbf{e}}_E$ . For a general  $\theta$ , both  $J_{\text{Bloch}}^{\parallel}$  and  $J_{\text{Bloch}}^{\perp}$  are nonzero at small  $E$  and decay to zero at large  $E$ , as shown in Figs. 2(a)–2(d). However, the crossover from the small- $E$  to the large- $E$  regimes is only weakly dependent on  $\theta$  for  $J_{\text{Bloch}}^{\parallel}$ , while  $J_{\text{Bloch}}^{\perp}$  features strong anisotropy in this crossover behavior.  $J_{\text{geom}}$  also features strong anisotropy; the residual current at

large  $E$  diverges near  $30^\circ$ ,  $90^\circ$ ,  $150^\circ$ ,  $210^\circ$ ,  $270^\circ$ , and  $330^\circ$ . The two transverse currents are distinguishable by their behavior under  $\mathbf{E}$ -inversion;  $J_{\text{Bloch}}^\perp$  is even under  $\mathbf{E}$ -inversion, while  $J_{\text{geom}}$  is odd under  $\mathbf{E}$ -inversion [52].

To observe geometric oscillations, at least three requirements must be met: (i) the lattice constant must be large enough that the onset of geometric oscillations  $eEL\tau/\hbar > 1$  can be achieved with reasonable field strengths; (ii) the bandwidth must be small enough compared to the band gaps that Zener tunneling can be neglected,  $eEL \ll \mathcal{E}_{\text{gap}}^2/\mathcal{E}_{\text{width}}$  [47]; and (iii) the bands of interest must carry significant Berry curvature. All of these requirements can be met with superlattice materials that host flat bands. For example, twisted bilayer graphene aligned on hexagonal boron nitride, which induces a  $\sigma_z$  mass on the bottom graphene layer of about 30 meV [53–55], is a promising candidate. At  $\theta = 1.0^\circ$  with  $L \approx 140 \text{ \AA}$ , each valley carries a Chern band with  $C = \pm 1$  and  $\mathcal{E}_{\text{gap}}^2/\mathcal{E}_{\text{width}} \approx 5.5 \text{ meV}$ . For a typical relaxation time of 1 ps [56], the onset of geometric oscillations requires  $E \approx 0.5 \text{ kV/cm}$ , which is both experimentally feasible and well below the Zener limit. Beyond twisted bilayer graphene, the many recently discovered twistrionic materials are promising candidates. For example, it is possible to increase the valley Chern number in graphene-based flat bands by stacking more layers, which would enhance the nonlinear Hall current [57–61]. At small fields, the second-order nonlinear Hall effect has already been observed in twisted bilayer and double bilayer graphene [62–64]. It is reasonable to speculate that at larger fields, the onset of geometric oscillations might be observable in these platforms.

In closing, we comment on several possible extensions. Of immediate relevance is augmenting the present discussion to include Zener tunneling, in which Berry phase effects are known to appear [65,66]. It would also be interesting to consider the signatures of geometric oscillations in experimental probes beyond transport measurements, such as in optical setups [10,67]. Finally, Bloch oscillations have been extensively studied both experimentally and theoretically in non-solid-state media, including in cold-atoms systems [68] and in photonic waveguides [69–72]. Perhaps these platforms can also host geometric oscillations once the right ingredients have been added to proliferate the Berry curvature.

We thank Christophe De Beule for valuable conversations. This work is supported by the Department of Energy under Grant No. DE-FG02-84ER45118. V. T. P. acknowledges further support from the P. D. Soros Fellowship for New Americans and the National Science Foundation's Graduate Research Fellowships Program.

- 
- [1] R. Tsu, *Superlattice to Nanoelectronics* (Elsevier Science, New York, 2005).  
 [2] E. Y. Andrei and A. H. MacDonald, Graphene bilayers with a twist, *Nat. Mater.* **19**, 1265 (2020).

- [3] K. F. Mak and J. Shan, Semiconductor moiré materials, *Nat. Nanotechnol.* **17**, 686 (2022).  
 [4] E. Suárez Morell, J. D. Correa, P. Vargas, M. Pacheco, and Z. Barticevic, Flat bands in slightly twisted bilayer graphene: Tight-binding calculations, *Phys. Rev. B* **82**, 121407 (R) (2010).  
 [5] R. Bistritzer and A. H. MacDonald, Moiré bands in twisted double-layer graphene, *Proc. Natl. Acad. Sci. U.S.A.* **108**, 12233 (2011).  
 [6] P. Moon and M. Koshino, Energy spectrum and quantum Hall effect in twisted bilayer graphene, *Phys. Rev. B* **85**, 195458 (2012).  
 [7] Z. Zhang, Y. Wang, K. Watanabe, T. Taniguchi, K. Ueno, E. Tutuc, and B. J. LeRoy, Flat bands in twisted bilayer transition metal dichalcogenides, *Nat. Phys.* **16**, 1093 (2020).  
 [8] S. Lisi, X. Lu, T. Benschop, T. A. de Jong, P. Stepanov, J. R. Duran, F. Margot, I. Cucchi, E. Cappelli, A. Hunter *et al.*, Observation of flat bands in twisted bilayer graphene, *Nat. Phys.* **17**, 189 (2021).  
 [9] K. Leo, P. H. Bolivar, F. Brüggemann, R. Schwedler, and K. Köhler, Observation of Bloch oscillations in a semiconductor superlattice, *Solid State Commun.* **84**, 943 (1992).  
 [10] J. Feldmann, K. Leo, J. Shah, D. A. B. Miller, J. E. Cunningham, T. Meier, G. von Plessen, A. Schulze, P. Thomas, and S. Schmitt-Rink, Optical investigation of Bloch oscillations in a semiconductor superlattice, *Phys. Rev. B* **46**, 7252 (1992).  
 [11] T. Dekorsy, R. Ott, H. Kurz, and K. Köhler, Bloch oscillations at room temperature, *Phys. Rev. B* **51**, 17275 (1995).  
 [12] A. M. Bouchard and M. Luban, Bloch oscillations and other dynamical phenomena of electrons in semiconductor superlattices, *Phys. Rev. B* **52**, 5105 (1995).  
 [13] A. A. Ignatov, E. Schomburg, J. Grenzer, K. Renk, and E. Dodin, THz-field induced nonlinear transport and dc voltage generation in a semiconductor superlattice due to Bloch oscillations, *Z. Phys. B Condens. Matter* **98**, 187 (1995).  
 [14] G. H. Wannier, Wave functions and effective Hamiltonian for Bloch electrons in an electric field, *Phys. Rev.* **117**, 432 (1960).  
 [15] E. E. Mendez and G. Bastard, Wannierstark ladders and Bloch oscillations in superlattices, *Phys. Today* **46**, No. 6, 34 (1993).  
 [16] A. Fahimniya, Z. Dong, E. I. Kiselev, and L. Levitov, Synchronizing Bloch-Oscillating Free Carriers in Moiré Flat Bands, *Phys. Rev. Lett.* **126**, 256803 (2021).  
 [17] T. Vakhtel, D. Oriekhov, and C. Beenakker, Bloch oscillations in the magnetoconductance of twisted bilayer graphene, *Phys. Rev. B* **105**, L241408 (2022).  
 [18] F. Wu, T. Lovorn, E. Tutuc, I. Martin, and A. H. MacDonald, Topological Insulators in Twisted Transition Metal Dichalcogenide Homobilayers, *Phys. Rev. Lett.* **122**, 086402 (2019).  
 [19] Y. Gao, Y. Zhang, and D. Xiao, Tunable Layer Circular Photogalvanic Effect in Twisted Bilayers, *Phys. Rev. Lett.* **124**, 077401 (2020).  
 [20] P. A. Pantaleón, T. Low, and F. Guinea, Tunable large berry dipole in strained twisted bilayer graphene, *Phys. Rev. B* **103**, 205403 (2021).

- [21] T. Devakul, V. Crépel, Y. Zhang, and L. Fu, Magic in twisted transition metal dichalcogenide bilayers, *Nat. Commun.* **12**, 1 (2021).
- [22] C.-P. Zhang, J. Xiao, B. T. Zhou, J.-X. Hu, Y.-M. Xie, B. Yan, and K. T. Law, Giant nonlinear hall effect in strained twisted bilayer graphene, *Phys. Rev. B* **106**, L041111 (2022).
- [23] H. M. Price and N. R. Cooper, Mapping the Berry curvature from semiclassical dynamics in optical lattices, *Phys. Rev. A* **85**, 033620 (2012).
- [24] M. Wimmer, H. M. Price, I. Carusotto, and U. Peschel, Experimental measurement of the Berry curvature from anomalous transport, *Nat. Phys.* **13**, 545 (2017).
- [25] D. Emin and C. F. Hart, Existence of Wannier-Stark localization, *Phys. Rev. B* **36**, 7353 (1987).
- [26] L. Kleinman, Comment on “Existence of Wannier-Stark localization”, *Phys. Rev. B* **41**, 3857 (1990).
- [27] D. A. Page and E. Brown, Comment on “Existence of Wannier-Stark localization”, *Phys. Rev. B* **43**, 2423 (1991).
- [28] J. Leo and A. MacKinnon, Comment on “Existence of Wannier-Stark localization”, *Phys. Rev. B* **43**, 5166 (1991).
- [29] G. Nenciu, Dynamics of band electrons in electric and magnetic fields: Rigorous justification of the effective Hamiltonians, *Rev. Mod. Phys.* **63**, 91 (1991).
- [30] L. Esaki and R. Tsu, Superlattice and negative differential conductivity in semiconductors, *IBM J. Res. Dev.* **14**, 61 (1970).
- [31] M.-C. Chang and Q. Niu, Berry Phase, Hyperorbits, and the Hofstadter Spectrum, *Phys. Rev. Lett.* **75**, 1348 (1995).
- [32] M.-C. Chang and Q. Niu, Berry phase, hyperorbits, and the Hofstadter spectrum: Semiclassical dynamics in magnetic Bloch bands, *Phys. Rev. B* **53**, 7010 (1996).
- [33] D. Xiao, M.-C. Chang, and Q. Niu, Berry phase effects on electronic properties, *Rev. Mod. Phys.* **82**, 1959 (2010).
- [34] M. Saitoh, Stark ladders in solids, *J. Phys. C* **5**, 914 (1972).
- [35] M. Grifoni and P. Hänggi, Driven quantum tunneling, *Phys. Rep.* **304**, 229 (1998).
- [36] T. Hartmann, F. Keck, H. Korsch, and S. Mossmann, Dynamics of Bloch oscillations, *New J. Phys.* **6**, 2 (2004).
- [37] D. Witthaut, F. Keck, H. Korsch, and S. Mossmann, Bloch oscillations in two-dimensional lattices, *New J. Phys.* **6**, 41 (2004).
- [38] We should point out that in order for the derivative with respect to  $\mathbf{k}$  to be defined, we must regard  $\mathbf{k}$  to be a continuous variable, which corresponds to the limit of  $\mathcal{N} \rightarrow \infty$ . Throughout this work, we assume this limit implicitly; thus, we use  $\mathcal{N}^{-1} \sum_{\mathbf{k}}$  and  $V_{\text{BZ}}^{-1} \int d^2\mathbf{k}$  interchangeably.
- [39] See Supplemental Material at <http://link.aps.org/supplemental/10.1103/PhysRevLett.130.266601> for a discussion of the Wannier-Stark formalism, a derivation of transport properties using Boltzmann equation, a derivation of numerical derivatives, and a calculation on twisted bilayer graphene.
- [40] C. Zener, Non-adiabatic crossing of energy levels, *Proc. R. Soc. A* **137**, 696 (1932).
- [41] E. O. Kane, Theory of tunneling, *J. Appl. Phys.* **32**, 83 (1961).
- [42] H. Fukuyama, R. A. Bari, and H. C. Fogedby, Tightly bound electrons in a uniform electric field, *Phys. Rev. B* **8**, 5579 (1973).
- [43] A. Di Carlo, P. Vogl, and W. Pötz, Theory of Zener tunneling and Wannier-Stark states in semiconductors, *Phys. Rev. B* **50**, 8358 (1994).
- [44] F. Beltram, F. Capasso, D. L. Sivco, A. L. Hutchinson, S.-N. G. Chu, and A. Y. Cho, Scattering-Controlled Transmission Resonances and Negative Differential Conductance by Field-Induced Localization in Superlattices, *Phys. Rev. Lett.* **64**, 3167 (1990).
- [45] N. Marzari and D. Vanderbilt, Maximally localized generalized Wannier functions for composite energy bands, *Phys. Rev. B* **56**, 12847 (1997).
- [46] A. Pippard, *The Dynamics of Conduction Electrons*, Documents on Modern Physics (Gordon and Breach, New York, 1965).
- [47] N. W. Ashcroft and N. D. Mermin, *Solid State Physics* (Cengage Learning, Andover, 1976).
- [48] It is in principle possible to observe oscillatory currents if the sample is clean enough that the scattering time is at least several times the period of the oscillations. However, these transient signatures are more difficult to achieve experimentally, so we focus instead on steady-state effects in this work. We leave the analysis of the time-domain signals to future work.
- [49] T. Low, Y. Jiang, and F. Guinea, Topological currents in black phosphorus with broken inversion symmetry, *Phys. Rev. B* **92**, 235447 (2015).
- [50] I. Sodemann and L. Fu, Quantum Nonlinear Hall Effect Induced by Berry Curvature Dipole in Time-Reversal Invariant Materials, *Phys. Rev. Lett.* **115**, 216806 (2015).
- [51] A. Sibille, J. F. Palmier, H. Wang, and F. Mollot, Observation of Esaki-Tsu Negative Differential Velocity in GaAs/AlAs Superlattices, *Phys. Rev. Lett.* **64**, 52 (1990).
- [52] There is a potential confusion in this terminology.  $\mathbf{J}_{\text{Bloch}}^{\perp}$  is odd under  $\mathbf{E}$ -inversion, while  $\mathbf{J}_{\text{geom}}$  is even under  $\mathbf{E}$ -inversion. However, since the basis vector  $\hat{\mathbf{e}}_{\mathbf{E}}$  is odd under  $\mathbf{E}$ -inversion, the components  $J_{\text{Bloch}}^{\perp}$  and  $J_{\text{geom}}$  obey the opposite symmetry constraints to their vectors.
- [53] M. Koshino, N. F. Q. Yuan, T. Koretsune, M. Ochi, K. Kuroki, and L. Fu, Maximally Localized Wannier Orbitals and the Extended Hubbard Model for Twisted Bilayer Graphene, *Phys. Rev. X* **8**, 031087 (2018).
- [54] S. Lisi, X. Lu, T. Benschop, T. A. de Jong, P. Stepanov, J. R. Duran, F. Margot, I. Cucchi, E. Cappelli, A. Hunter *et al.*, Observation of flat bands in twisted bilayer graphene, *Nat. Phys.* **17**, 189 (2021).
- [55] M. Long, P. A. Pantaleón, Z. Zhan, F. Guinea, J. Á. Silva-Guillén, and S. Yuan, An atomistic approach for the structural and electronic properties of twisted bilayer graphene-boron nitride heterostructures, *npj Comput. Mater.* **8**, 73 (2022).
- [56] J. M. Dawlaty, S. Shivaraman, M. Chandrashekhara, F. Rana, and M. G. Spencer, Measurement of ultrafast carrier dynamics in epitaxial graphene, *Appl. Phys. Lett.* **92**, 042116 (2008).
- [57] Y.-H. Zhang, D. Mao, Y. Cao, P. Jarillo-Herrero, and T. Senthil, Nearly flat Chern bands in moiré superlattices, *Phys. Rev. B* **99**, 075127 (2019).
- [58] N. R. Chebrolov, B. L. Chittari, and J. Jung, Flat bands in twisted double bilayer graphene, *Phys. Rev. B* **99**, 235417 (2019).



- [59] M. Koshino, Band structure and topological properties of twisted double bilayer graphene, *Phys. Rev. B* **99**, 235406 (2019).
- [60] J. Liu, Z. Ma, J. Gao, and X. Dai, Quantum Valley Hall Effect, Orbital Magnetism, and Anomalous Hall Effect in Twisted Multilayer Graphene Systems, *Phys. Rev. X* **9**, 031021 (2019).
- [61] F. Haddadi, Q. Wu, A. J. Kruchkov, and O. V. Yazyev, Moiré flat bands in twisted double bilayer graphene, *Nano Lett.* **20**, 2410 (2020).
- [62] J. Duan, Y. Jian, Y. Gao, H. Peng, J. Zhong, Q. Feng, J. Mao, and Y. Yao, Giant Second-Order Nonlinear Hall Effect in Twisted Bilayer Graphene, *Phys. Rev. Lett.* **129**, 186801 (2022).
- [63] S. Sinha, P. C. Adak, A. Chakraborty, K. Das, K. Debnath, L. Sangani, K. Watanabe, T. Taniguchi, U. V. Waghmare, A. Agarwal *et al.*, Berry curvature dipole senses topological transition in a moiré superlattice, *Nat. Phys.* **18**, 765 (2022).
- [64] A. Chakraborty, K. Das, S. Sinha, P. C. Adak, M. M. Deshmukh, and A. Agarwal, Nonlinear anomalous Hall effects probe topological phase-transitions in twisted double bilayer graphene, *2D Mater.* **9**, 045020 (2022).
- [65] K. Sota, N. Naoto, and M. Takahiro, Nonreciprocal Landau-Zener tunneling, *Commun. Phys.* **3**, 63 (2020).
- [66] Presumably, the many-band formalism would also lift the restriction that the band of interest must be Chern trivial as assumed in this work, since in such a more general framework, only the sum of all Chern numbers needs to be zero.
- [67] K. Leo, Interband optical investigation of Bloch oscillations in semiconductor superlattices, *Semicond. Sci. Technol.* **13**, 249 (1998).
- [68] M. Ben Dahan, E. Peik, J. Reichel, Y. Castin, and C. Salomon, Bloch Oscillations of Atoms in an Optical Potential, *Phys. Rev. Lett.* **76**, 4508 (1996).
- [69] U. Peschel, T. Pertsch, and F. Lederer, Optical Bloch oscillations in waveguide arrays, *Opt. Lett.* **23**, 1701 (1998).
- [70] R. Morandotti, U. Peschel, J. S. Aitchison, H. S. Eisenberg, and Y. Silberberg, Experimental Observation of Linear and Nonlinear Optical Bloch Oscillations, *Phys. Rev. Lett.* **83**, 4756 (1999).
- [71] R. Sapienza, P. Costantino, D. Wiersma, M. Ghulinyan, C. J. Oton, and L. Pavesi, Optical Analogue of Electronic Bloch Oscillations, *Phys. Rev. Lett.* **91**, 263902 (2003).
- [72] S. Longhi, Bloch Oscillations in Complex Crystals with  $\mathcal{PT}$  Symmetry, *Phys. Rev. Lett.* **103**, 123601 (2009).